Can the Four-Coordinated, Penta-Valent Oxygen in Hydroxide Water Clusters Be Detected through Experimental Vibrational Spectroscopy?

Xiaohu Li, Virginia E. Teige, and Srinivasan S. Iyengar*

Department of Chemistry, Indiana University, 800 E. Kirkwood Ave, Bloomington, Indiana 47405

Received: January 11, 2007; In Final Form: March 19, 2007

In this study, we construct the hydroxide water cluster, $OH^-(H_2O)_6$, that (a) could support a stable hydroxide ion with a four-coordinated (pentavalent) hydroxide oxygen and (b) displays hydroxide ion migration. We study the energetic stability and dynamical evolution of the system at different internal temperatures and analyze the corresponding "dynamically averaged" vibrational density of states to discuss the conditions under which the pentavalent oxygen may be observed using vibrational action spectroscopy. We also provide an alternate hydroxide migration mechanism.

I. Introduction

The structure, dynamics, and spectroscopy of protonated, unprotonated, and hydroxide water clusters have remained an important challenge with fundamental implications.[1−23] Although proton transfer is widely accepted to follow the "Grotthuss" mechanism,[21] the "hole hopping" hydroxide transfer process[17] has been challenged[2,3] and the existence and role of a four-coordinated (pentavalent) hydroxide oxygen as an intermediate in hydroxide transport in aqueous phase is debated.[2−4]

In previous theoretical studies,[3] Car Parrinello ab initio molecular dynamics simulations[24−26] with imaginary time path integrals, to account for equilibrium nuclear quantum effects, and BLYP density functional, were employed to probe the hydroxide transfer mechanism in the aqueous phase. It was found[3] that a stable four-coordinated $OH^-(H_2O)_4$ complex converts to $OH^-(H_2O)_3$ and thermal fluctuations of the hydroxide-water hydrogen bond and first solvation shell water cause a proton transfer to the central OH^-. This results in a first solvation shell water converting to hydroxide and thus facilitating transport. The $OH^-(H_2O)_4$ was thus proposed as central whose transformation to $OH^-(H_2O)_3$ was considered rate determining. However, subsequent adiabatic ab initio Born Oppenheimer dynamics studies[4] with similar basis sets and using a wider range of density functionals, but without nuclear quantum effects, suggest that $OH^-(H_2O)_3$ was the prominent species in the hydroxide migration process. The four-coordinated species is also seen in the dynamics results in ref 4, but to a much lesser extent as compared to the three-coordinated species. Thus the authors in ref 4 conclude that the traditional hole hopping mechanism has substantial validity. If a four-coordinated oxygen intermediate exists and can be detected experimentally, this would provide valuable insight into the hydroxide migration mechanism. Furthermore, this would be of fundamental chemical interest on account of the presence of five groups (the four nonbonded water molecules and the hydroxyl hydrogen) around a central oxygen.

In this study, we construct the smallest hydroxide water cluster, $OH^-(H_2O)_6$, in gas-phase that (a) could support a stable hydroxide ion with a four-coordinated hydroxide oxygen[22] and (b) display hydroxide ion migration. We study the energetic stability and dynamical evolution of the system at different internal temperatures and analyze the corresponding "dynamically averaged" vibrational density of states inclusive of nuclear quantum effects. Recent studies by one of us[16,27] has revealed that dynamical effects are critical in obtaining vibrational density of states in agreement with experiment for fluxional systems such as protonated water clusters.[16] The effect of dynamics on vibrational spectra and electronic spectra has also been demonstrated for HO_2−water clusters.[27] As we see in this contribution, dynamical effects and conformational averaging also play an important role on the vibrational spectrum of hydroxide water clusters. We also provide an alternate hydroxide migration mechanism as part of our study. Our tool includes ab initio molecular dynamics (both Born Oppenheimer and extended Lagrangian techniques are used here on account of the subtle differences between the results in refs 3 and 4) as well as single point optimization and harmonic frequency calculations using DFT and post-Hartree−Fock methods. Our aim is to use the dynamically averaged vibrational signatures to provide a spectroscopic probe for the existence of a four-coordinated, pentavalent central oxygen. Since clusters of the size described in this study, are accessible to vibrational action spectrum experiments,[1,28] our predictions of the hydroxide transfer pathways and dynamically averaged vibrational spectra can be tested. This paper is organized as follows: In section II, the computational methods used are briefly outlined. In section III, our structural and spectroscopic results are discussed from both static and dynamic studies. Conclusions are given in section IV.

II. Computational Methods

The simulations conducted in this study use ab initio molecular dynamics (AIMD) techniques, Born−Oppenheimer molecular dynamics (BOMD),[29−32] and the atom-centered density matrix propagation (ADMP)[33−38] extended Lagrangian technique,[24,39,40] as implemented within the Gaussian series of electronic structure codes.[41] These simulations utilize the B3LYP hybrid density functional with double-ζ polarized-diffused 6-31+G** basis, as suggested from previous studies[16,37,38,42,43] on similar systems. In addition, geometry optimization and

* To whom correspondence should be addressed. E-mail: iyengar@indiana.edu.

10.1021/jp070241u CCC: $37.00
Published on Web 05/15/2007

frequency calculations at the B3LYP level and post-Hartree Fock MP2 level using the triple-ζ 6-311++G** Gaussian basis are also performed to confirm the results. Nuclear quantum effects for all atoms are included in our AIMD calculations through a Harmonic correction factor[44] that is exact in the limit where the dipole operator is a linear combination of degrees of freedom that are well described by a harmonic Hamiltonian. A time step of 0.5 fs was chosen for all BOMD dynamics studies, whereas a fictitious mass-tensor scaling value of 0.25 amu bohr^2 ($\approx$180 a.u.) and a time-step of 0.1 fs was used for ADMP. All AIMD simulations conducted here are microcanonical (NVE).

ADMP is an extended Lagrangian[24,39,40] form of AIMD that has been described in detail elsewhere.[33−37,45] The accuracy of this approach has been demonstrated through the treatment of several interesting problems.[16,27,35,37,38,45] Perhaps the most notable among these applications include: (a) a recent demonstration[16,27] that dynamical effects are critical in obtaining good vibrational spectroscopic properties of flexible systems[16,27] such as those encountered in this paper and (b) the prediction of the "amphiphilic" nature of the hydrated proton.[16,38,46]

In the present study, vibrational spectra were computed in two different ways. To obtain dynamically averaged vibrational spectra, Fourier-transform of the velocity and dipole autocorrelation functions were computed from AIMD simulations. Quantum nuclear corrections are added through a Harmonic multiplicative correction factor for the Fourier transform of the time-correlation function: $C(\omega) \times (\beta\hbar\omega)/(1 - \exp[-\beta\hbar\omega])$, which has been shown to provide results in good agreement with the semiclassical forward−backward propagation scheme.[44] To evaluate the role of finite temperature in AIMD and to help compare with static nuclear descriptions, harmonic frequencies were obtained for the inherent AIMD structures (or isomeric forms) using DFT and MP2 with triple-ζ split valence, polarized diffuse basis 6-311++G**. These isomeric forms of the dynamical simulations are obtained through geometry optimization at B3LYP levels from snapshots from the AIMD trajectory procured at intervals of $\approx$550 fs (see section III below). The geometry optimizations are then confirmed through MP2 frequency calculations.

III. Results and Discussion

The starting point for our studies is the two stable structures shown in Figure 1, panels a and b. Figure 1b shows a structure with a four-coordinated hydroxide oxygen (C_2 symmetric), and Figure 1a has a more conventional tetrahedrally coordinated central oxygen (C_{3v}). Thus, these structures represent the two distinct families of three- and four-coordinated hydroxide systems. Both structures have secondary shell water molecules that stabilize the inner shell interactions and play an important role in hydroxide migration. Calculations at the B3LYP and MP2 levels indicate the four-coordinated species to be more stable (by 0.4 kcal/mol in B3LYP and by 0.9 kcal/mol in MP2). Harmonic frequencies for these structures are presented in Figure 1c with critical differences corresponding to the first solvation shell hydrogen bond stretch in the 2700−3500 cm^{-1} region. Figure 1c reveals that the B3LYP frequencies are uniformly red-shifted with respect to MP2, but the relative positions of these peaks are similar in both cases. (No scaling factors are employed in the current study.) Both methods consistently reveal the important differences between the two configurations. For the C_2 structure, the two peaks around 3100 cm^{-1} for B3LYP represent symmetric and asymmetric linear combinations of the four internal first shell hydrogen bonds. It should be noted that the first shell water molecules at opposite ends for C_2 have the same hydrogen bond length. The peak around 2700 cm^{-1} in C_{3v} corresponds to the OH stretch from the three identical neighboring hydrogen bonds.

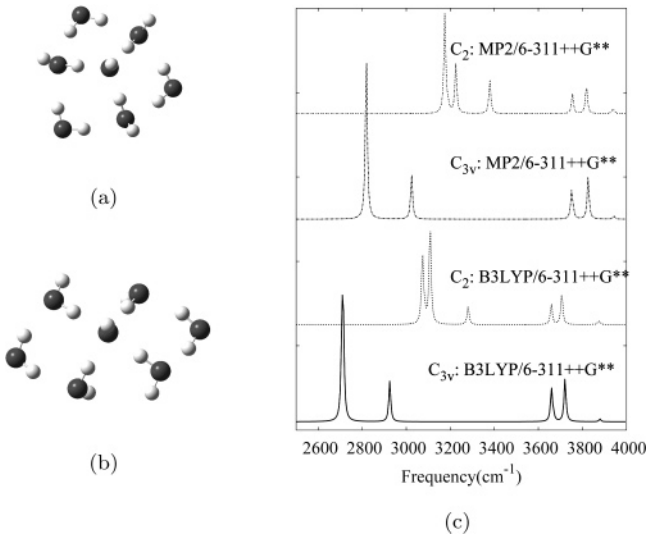

Figure 1. Three-coordinated (C_{3v} structure; panel a) and four-coordinated (C_2 symmetric; panel b) starting structures for AIMD simulations. The distance between the hydroxide oxygen and first shell water oxygens for the C_{3v} structure is 2.6 Å, whereas that for the C_2 structure is 2.7 Å. Figure (c): Geometry optimized harmonic frequencies for these structures.

TABLE 1: Summary of AIMD Simulations Performed for Structural and Spectroscopic Analysis

starting geometry	temp. (K)	cm^{-1a}	method	simulation time (T), (ps)	$1/(2T)^b$ (cm^{-1})
C_{3v}	220 ± 37.5	4390	BOMD	38.6	0.4
		4390	ADMP	5.5	3.0
	113 ± 17	2190	BOMD	29.8	0.6
		2190	ADMP	7.7	2.2
	56 ± 8	1150	BOMD	13.8	1.2
	29 ± 4	575	BOMD	9.7	1.7
C_2	220 ± 30	4390	BOMD	30.1	0.6
		4390	ADMP	10	1.7
	110 ± 17	2190	BOMD	22.4	0.8
		2190	ADMP	9.4	1.8
	57 ± 9	1150	BOMD	14.1	1.2
	29 ± 4	575	BOMD	13.8	1.2

[a] Approximate average photon energy: The average internal temperature is converted to wave-numbers here for an idea of the amount of energy transferred from a single photon or a group of photons that would give rise to this internal temperature for the six-water hydroxide cluster system during an action spectrum experiment. [b] Based on Shannon sampling theorem,[47] we estimate here the uncertainty in frequency, when the dynamics is utilized to compute vibrational spectra.

Would the difference in these fundamental stretch frequencies be useful in detecting a pentavalent oxygen spectroscopically? To understand if these spectral features will remain in vibrational action spectrum experiments,[1,28] we simulate the finite temperature behavior of these clusters using AIMD. Toward this we consider four different constant energy simulations with different amounts of internal kinetic energies. These simulations each lead to trajectories that conserve the total energy and have different average temperatures (with fluctuations $\approx$ 10−15%) which are attainable experimentally. The simulations were conducted at approximately 29, 58, 110, and 220 K, starting from the C_2 and C_{3v} structures in Figure 1, panels a and b. Simulation details are in Table 1 and animations (mpg files) showing the dynamics can be found in the Supporting Information. The low temperatures (110 K and lower) are accessible to

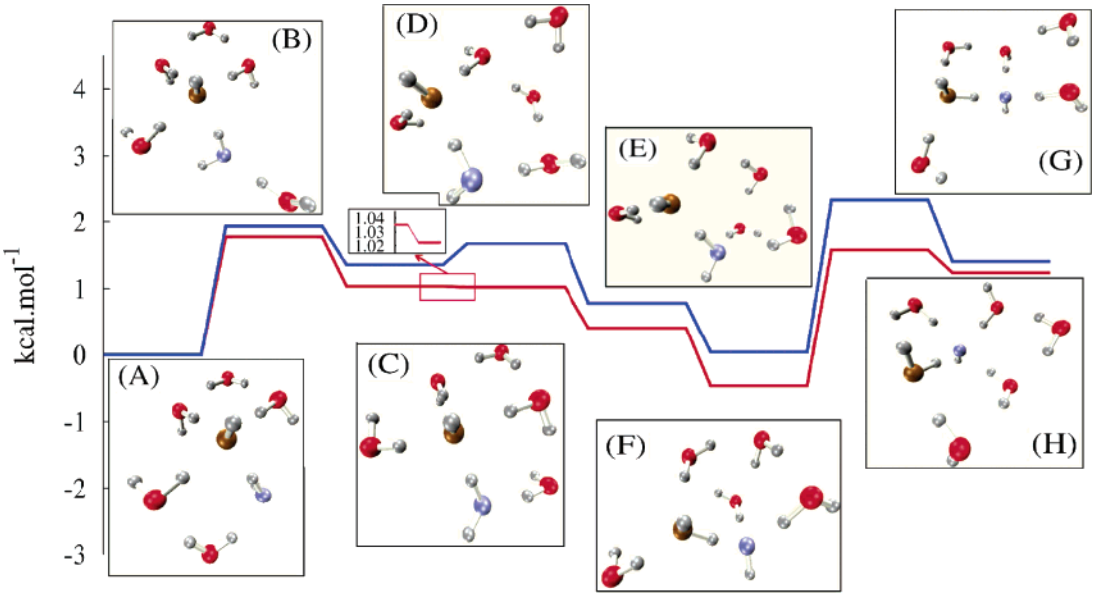

Figure 2. Structural evolution with energies obtained from geometry optimization of structures picked at intervals of ≈550 ps from AIMD (red lines, B3LYP; blue lines, MP2). Water oxygens are red, and hydrogens are grey. The initial hydroxide oxygen is brown. The atom shown in aquamarine starts as a water oxygen but loses a proton during dynamics to become a hydroxide (structures F−H).

single photon argon tagged action spectrum experiments[12] whereas the higher temperature of ≈220 K can be attained in some gas-phase multiphoton experiments.[28] The definition of temperature in our simulations is an internal temperature that is defined in terms of the total classical kinetic energy of the nuclei.

The structural evolution of the system inclusive of the various isomers (or inherent structures) sampled during the dynamics at 220 K are shown in Figure 2. Starting from the C_2 structure (A), the system evolves through accessible intermediates (B and C) into five-membered ring structures (D and E) that facilitate a proton hop and a resultant hydroxide migration eventually leading into another four-coordinated central hydroxide (H). The five-membered ring that supports the hydroxide through three water molecules donating hydrogen bonds (similar to that in the C_{3v} structure) seems central to this hydroxide transfer process. Figure 2 also illustrates a family of four-coordinated (A, B, C, and H) and three-coordinated structures (D−F). The importance of these two families of structures to the spectroscopy of the hydroxide water cluster is discussed further below. As noted above, the study in refs 3 and 4 indicates how hydroxide migration can occur in aqueous systems. Our study here shows that, even in the gas phase, small hydroxide water cluster can undergo hydroxide transport due to thermal fluctuation of first coordinate shell water and the four-coordinated species seems to have an important role.

As is to be expected based on our dynamical analysis, no single structure presented in Figure 2 completely dominates the vibrational spectrum at temperatures accessible to action spectrum experiments (100−250 K) due to the small energy differences between the accessible isomers. The harmonic vibrational spectral features in these isomers are very different as highlighted in Figure 3, panels a and b. (The B3LYP and MP2 results are qualitatively consistent in underlining this fluxional nature of the hydroxide water cluster system studied here.) There is a great deal of fluctuation in the 2000−3500 cm^{-1} range, and all peaks responsible for this fluctuation come from the internal hydrogen bonds in the cluster between hydroxide oxygen and neighboring water molecules. The hydrogen-bonded stretch at 3100 cm^{-1} for structure A is brought down to about 2600 cm^{-1} in C on account of the fact that three of the neighboring water-hydroxide oxygen distances in C are very similar and close to the tetrahedral neighboring oxygen−oxygen distance (about 0.1−0.2 Å shorter than for the penta-valent case). For the structures D−G, the hydroxide ion is shared by three neighboring water molecules, and this results in a strong 2600 cm^{-1} hydrogen bond stretch signature peak. Structure H resembles the geometry in structure C for the B3LYP case and they have similar harmonic frequencies.

To proceed further, we first note that an experimental measurement would yield an ensemble average of the spectroscopic features seen from all of the isomers. We use ab initio dynamics here to construct such an ensemble average. We have also considered a temperature-dependent Boltzmann average of the frequencies in Figure 2, but a Boltzmann average is purely based on the energetic stability of each isomer and does not include the entropic and an-harmonic contributions present in AIMD, since the latter samples the minimum energy points and surrounding regions. To construct the temperature dependent, dynamically averaged, vibrational spectrum, we consider the Fourier transform of the dipole correlation function[48−52] inclusive of nuclear quantum effects within the harmonic approximation (Figure 4). The dipole correlation function is constructed from the AIMD simulation results.[58] The signature peaks for the C_{3v} and C_2 geometries (2710 and 3100 cm^{-1} as seen in Figure 1c) are substantially weakened and broadened as a result of dynamical averaging at 220 K. At lower temperatures (110 K spectrum shown in Figure 4), the dynamics does indeed preserve features representing the four-coordinated central oxygen. The assignment of the various peaks found for the lower temperature spectrum in Figure 4 are as follows: The peak at ≈3800 cm^{-1} arises from the free OH stretch from the hydroxyl ion and the water molecules. The feature in the range 3550−3700 cm^{-1} arises from the second solvation shell water−water hydrogen bond stretch. The features at ≈3100 cm^{-1} arise from the OH stretch of water molecules that donate a hydrogen bond to a four-coordinated hydroxide ion, whereas the peaks at ≈2700 cm^{-1} arise from the OH stretch of water molecules that donate a hydrogen bond to a three-coordinated hydroxide ion. Thus, the lower temperature spectrum does indeed maintain a spectroscopic separation between the four- and three-coordinated structural features, thus leading to a temperature

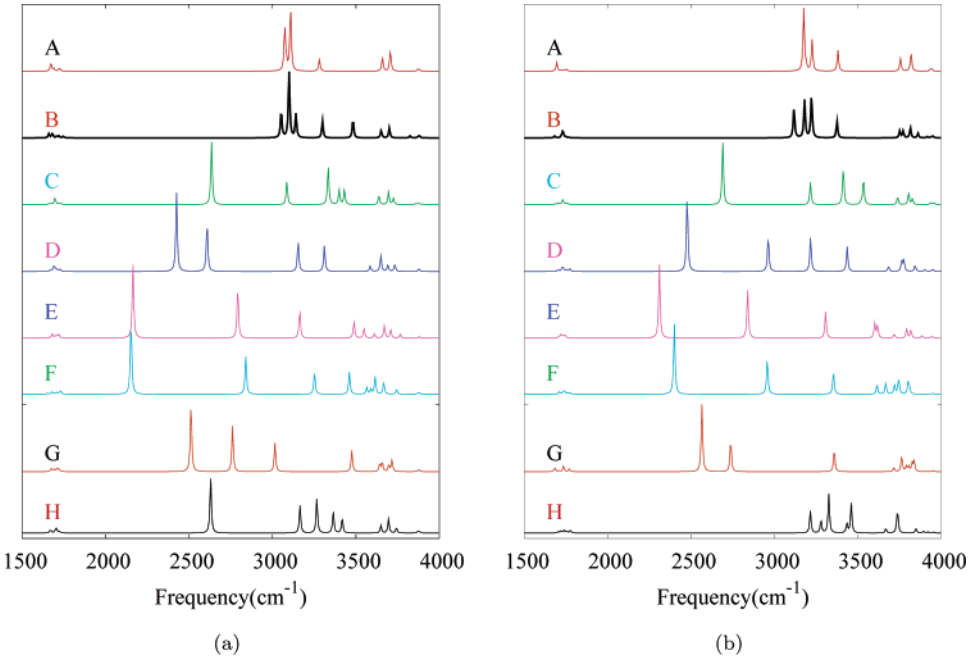

Figure 3. Harmonic frequencies at (a) the B3LYP and (b) MP2 levels of structures A−H.

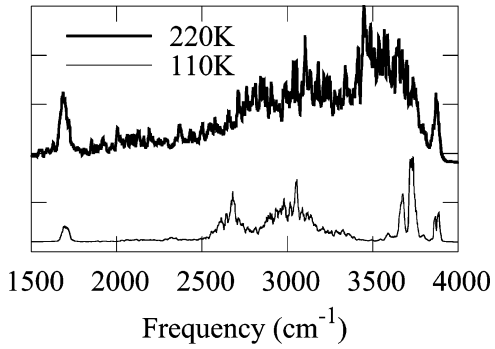

Figure 4. Fourier transform of dipole auto-correlation (FTDAC) with quantum nuclear corrections. The lower temperature spectrum shows critical features (see text) which get "averaged out" due to dynamics at higher temperature.

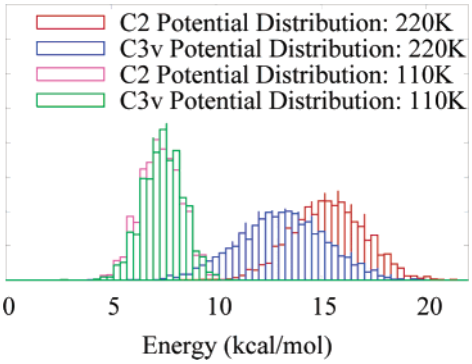

Figure 5. Distribution of potential energies sampled during dynamics. On the energy scale of panel c, structures A−H appear in the 0−2 kcal/mol region.

dependence of the vibrational spectrum. The reason for this temperature dependence in the spectrum is because the energy domains and regions of the potential surface sampled are different at different temperatures. Figure 5 shows that the lower temperature dynamics, on average, samples structures that are 5−10 kcal/mol above structure A, whereas the 220 K dynamics samples structures that are on average about 15 kcal/mol above the energy of structure A. (For comparison, it should be noted that all structures shown in Figure 2 are 0−2 kcal/mol above the energy of structure A.[59]) This difference in thermal sampling in conjunction with the polarizability of the hydroxide ion is responsible for the temperature-dependent effect found here.

Does the difference in potential energy sampling for different internal temperatures outlined above have a role to play in experimental vibrational action spectroscopy? Or is the difference in potential energy sampling essentially crippling in our calculations, on account of the computational expense involved in AIMD simulations as compared to when force-fields are employed? To address the second question (the first question is addressed in the next paragraph), we have considered portions of our relatively long 220 K [29.8 and 38.6 ps; see Table 1] and 110 K [22.4 and 30.1 ps; see Table 1] simulations and found essentially no change in the vibrational spectrum beyond 20 ps. This seems to indicate that the vibrational spectrum in Figure 4 has converged at ≈20 ps. Furthermore, it must be noted that simulations of the order of 20 ps have been known to provide well converged structural and vibrational properties for similar systems as those studied here.[4,16,27,53,54]

To consider if these simulations do have an experimental connection, we consider here two different kinds of experiments that are presently being employed by many groups to understand these kinds of clusters. In one set of experiments,[12] an argon tagged cluster is isolated using mass-spectrometry and then irradiated using a single IR photon of a given frequency. The photon energy, if absorbed, induces the cluster to undergo intracluster vibrational redistribution which may result in a suitable amount of energy being transferred into the argon−cluster weak interaction and the subsequent ejection of argon. This loss of argon could then be detected using a second mass-spectrometric measurement. Clearly, in this situation, the time scale of argon ejection and the intracluster vibrational redistribution is determined by (a) the amount of energy in the incident photon and (b) the structure of the cluster at the time when the photon is absorbed. These correspond to the initial structure in our simulations and the initial kinetic energy imparted to the molecules (which is converted to wave-numbers in Table 1 for comparison). It is important to note that the sampling of the potential energy surface (and hence the resultant spectrum) is

completely governed in this case by the two factors described above. In other words, the incident photon energy and the initial geometrical factors completely determine the dynamics both in the argon-tagged experimental action spectrum as well as the AIMD results presented here. Furthermore, these two factors also limit the region of conformational space that can be sampled, purely from (constant) energetic considerations.

In a second experimental situation,[28,55] which is also used by many groups to describe cluster vibrations, the internal vibrational energy of the system is elevated above the dissociation threshold by sequential absorption of many photons incident in a noncoherent fashion. The higher temperature AIMD simulations may be expected to simulate the predissociation dynamics in these experiments,[56] and there again the initial structure and initial kinetic energy dominate the sampling of the potential surface. As a result, we expect that, within the practical limitations of finite time AIMD, our lower internal temperature simulations may be closer to the argon tagged single-photon action spectrum experiments,[12] whereas our higher internal temperature AIMD simulations may be closer to multiphoton dissociation experiments.[28]

IV. Conclusions

Although the four-coordinated central oxygen is only one of the many structures that may be sampled during a finite temperature action spectrum experiment, our ab initio dynamics simulations indicate that it may still be possible to probe this structure by studying the temperature dependence of the vibrational spectrum at low enough temperatures for small clusters such as the one studied here. Our results suggest that single photon argon tagged action-spectrum experiments[7] and multiphoton action-spectrum experiments[28] may lead to different spectral results due to the higher internal temperature generated in a multiphoton experiment. The higher internal temperature leads to the sampling of different portions of the potential energy and hence different spectroscopic results. Based on the differences in the 2000−3500 cm^{-1} internal hydrogen bond stretch regions, it should be possible to probe the presence of a four-coordinated (pentavalent) central oxygen in the small hydroxide water cluster studied here.

With reference to previous hydroxide−water aqueous phase ab initio dynamics studies, we find that, for smaller gas-phase systems such as those studied here, the hydroxide migration pathways could be completely different from those seen in bulk-like systems. For example, here we find that a pathway exists where the hydroxide migrates through a five-membered ring intermediate which is apparently absent in the bulk-like simulations discussed in ref 3.

Acknowledgment. The research is supported by ACS-PRF and the IU-STARS (Indiana University Science, Technology And Research Scholars) program. We acknowledge Dr. David Moore from the Daniel M. Neumark Group for providing us with valuable insights on vibrational action spectrum experiments.

Supporting Information Available: Animations (mpg files) showing the dynamics. This material is available free of charge via the Internet at http://pubs.acs.org.

References and Notes

(1) Robertson, W. H.; Diken, E. G.; Price, E. A.; Shin, J.-W.; Johnson, M. A. *Science* **2003**, *299*, 1367−1372.
(2) Agmon, N. *Chem. Phys. Lett.* **2000**, *319*, 247−252.
(3) Tuckerman, M. E.; Marx, D.; Parrinello, M. *Nature* **2002**, *417*, 925−929.
(4) Asthagiri, D.; Pratt, L. R.; Kress, J. D.; Gomez, M. A. *Proc. Natl. Acad. Sci.* **2004**, *101*, 7229−7233.
(5) Shin, J.-W.; Hammer, N. I.; Diken, E. G.; Johnson, M. A.; Walters, R. S.; Jaeger, T. D.; Duncan, M. A.; Christie, R. A.; Jordan, K. D. *Science* **2004**, *304*, 1137−1140.
(6) Miyazaki, M.; Fujii, A.; Ebata, T.; Mikami, N. *Science* **2004**, *304*, 1134−1137.
(7) Headrick, J. M.; Diken, E. G.; Walters, R. S.; Hammer, N. I.; Christie, R. A.; Cui, J.; Myshakin, E. M.; Duncan, M. A.; Johnson, M. A.; Jordan, K. *Science* **2005**, *308*, 1765−1769.
(8) Zwier, T. S. *Science* **2004**, *304*, 1119−1120.
(9) Wu, C.-C.; Lin, C.-K.; Chang, H.-C.; Jiang, J.-C.; Kuo, J.-L.; Klein, M. L. *J. Chem. Phys.* **2005**, *122*, 074315.
(10) Chen, B.; Park, J. M.; Ivanov, I.; Tabacchi, G.; Klein, M. L.; Parrinello, M. *J. Am. Chem. Soc.* **2002**, *124*, 8534−8535.
(11) Diken, E. G.; Headrick, J. M.; Roscioli, J. R.; Bopp, J. C.; Johnson, M. A.; McCoy, A. B.; Huang, X.; Carter, S.; Bowman, J. M. *J. Phys. Chem. A* **2005**, *109*, 571−575.
(12) Diken, E. G.; Headrick, J. M.; Roscioli, J. R.; Bopp, J. C.; Johnson, M. A.; McCoy, A. B. *J. Phys. Chem. A* **2005**, *109*, 1487−1490.
(13) Price, E. A.; Robertson, W. H.; Diken, E. G.; Weddle, G. H.; Johnson, M. A. *Chem. Phys. Lett.* **2002**, *366*, 412.
(14) Xantheas, S. S. *J. Am. Chem. Soc.* **1995**, *117*, 10373−10380.
(15) McCoy, A. B.; Huang, X.; Carter, S.; Bowman, J. M. *J. Chem. Phys.* **2005**, *123* (6), 064317.
(16) Iyengar, S. S.; Petersen, M. K.; Day, T. J. F.; Burnham, C. J.; Teige, V. E.; Voth, G. A. *J. Chem. Phys.* **2005**, *123*, 084309.
(17) Bernal, J. D.; Fowler, R. H. *J. Chem. Phys.* **1933**, *1*, 515−548.
(18) Bakker, H. J.; Nienhuys, H. K. *Science* **2002**, *297*, 587.
(19) Eigen, M. *Angew. Chem., Int. Ed. Engl.* **1964**, *3*, 1.
(20) Zundel, G. *The Hydrogen Bond—Recent Developments in Theory and Experiments. II. Structure and Spectroscopy*; North-Holland: Amsterdam, 1976; pp 683−766.
(21) Agmon, N. *Chem. Phys. Lett.* **1995**, *244*, 456−462.
(22) Lee, H. M.; Tarkeshwar, P.; Kim, K. S. *J. Chem. Phys.* **2004**, *121*, 4657.
(23) Holland, P. M.; Castleman, A. W., Jr. *J. Chem. Phys.* **1980**, *72*, 5984−5990.
(24) Car, R.; Parrinello, M. *Phys. Rev. Lett.* **1985**, *55*, 2471.
(25) Remler, D. K.; Madden, P. A. *Mol. Phys.* **1990**, *70*, 921.
(26) Marx, D.; Hutter, J. *Ab Initio Molecular Dynamics: Theory and Implementation*; John vonNeumann Institute for Computing: Julich, 2000; Vol. 1, pp 301−449.
(27) Iyengar, S. S. *J. Chem. Phys.* **2005**, *123*, 084310.
(28) Moore, D. T.; Oomens, J.; van der Meer, L.; von Helden, G.; Meijer, G.; Valle, J.; Marshall, A. G.; Eyler, J. R. *ChemPhysChem* **2004**, *5*, 740−743.
(29) Wang, I. S. Y.; Karplus, M. *J. Am. Chem. Soc.* **1973**, *95*, 8160.
(30) Leforestier, C. *J. Chem. Phys.* **1978**, *68*, 4406.
(31) Bolton, K.; Hase, W. L.; Peslherbe, G. H. *Direct Dynamics of Reactive Systems*; World Scientific: Singapore, 1998; p 143.
(32) Payne, M. C.; Teter, M. P.; Allan, D. C.; Arias, T. A.; Joannopoulos, J. D. *Rev. Mod. Phys.* **1992**, *64*, 1045.
(33) Schlegel, H. B.; Millam, J. M.; Iyengar, S. S.; Voth, G. A.; Daniels, A. D.; Scuseria, G. E.; Frisch, M. J. *J. Chem. Phys.* **2001**, *114*, 9758.
(34) Iyengar, S. S.; Schlegel, H. B.; Millam, J. M.; Voth, G. A.; Scuseria, G. E.; Frisch, M. J. *J. Chem. Phys.* **2001**, *115*, 10291.
(35) Schlegel, H. B.; Iyengar, S. S.; Li, X.; Millam, J. M.; Voth, G. A.; Scuseria, G. E.; Frisch, M. J. *J. Chem. Phys.* **2002**, *117*, 8694.
(36) Iyengar, S. S.; Schlegel, H. B.; Voth, G. A.; Millam, J. M.; Scuseria, G. E.; Frisch, M. J. *Isr. J. Chem.* **2002**, *42*, 191−202.
(37) Iyengar, S. S.; Frisch, M. J. *J. Chem. Phys.* **2004**, *121*, 5061.
(38) Iyengar, S. S.; Day, T. J. F.; Voth, G. A. *Int. J. Mass Spectrometry* **2005**, *241*, 197−204.
(39) Andersen, H. C. *J. Chem. Phys.* **1980**, *72*, 2384−2393.
(40) Parrinello, M.; Rahman, A. *Phys. Rev. Lett.* **1980**, *45*, 1196−1199.
(41) Frisch, M. J.; Trucks, G. W.; Schlegel, H. B.; Scuseria, G. E.; Robb, M. A.; Cheeseman, J. R.; Montgomery, J. A., Jr.; Vreven, T.; Kudin, K. N.; Burant, J. C.; Millam, J. M.; Iyengar, S. S.; Tomasi, J.; Barone, V.; Mennucci, B.; Cossi, M.; Scalmani, G.; Rega, N.; Petersson, G. A.; Nakatsuji, H.; Hada, M.; Ehara, M.; Toyota, K.; Fukuda, R.; Hasegawa, J.; Ishida, M.; Nakajima, T.; Honda, Y.; Kitao, O.; Nakai, H.; Klene, M.; Li, X.; Knox, J. E.; Hratchian, H. P.; Cross, J. B.; Bakken, V.; Adamo, C.; Jaramillo, J.; Gomperts, R.; Stratmann, R. E.; Yazyev, O.; Austin, A. J.; Cammi, R.; Pomelli, C.; Ochterski, J. W.; Ayala, P. Y.; Morokuma, K.; Voth, G. A.; Salvador, P.; Dannenberg, J. J.; Zakrzewski, V. G.; Dapprich, S.; Daniels, A. D.; Strain, M. C.; Farkas, O.; Malick, D. K.; Rabuck, A. D.; Raghavachari, K.; Foresman, J. B.; Ortiz, J. V.; Cui, Q.; Baboul, A. G.; Clifford, S.; Cioslowski, J.; Stefanov, B. B.; Liu, G.; Liashenko, A.; Piskorz, P.; Komaromi, I.; Martin, R. L.; Fox, D. J.; Keith, T.; Al-Laham, M. A.; Peng, C. Y.; Nanayakkara, A.; Challacombe, M.; Gill, P. M. W.; Johnson, B.; Chen, W.; Wong, M. W.; Gonzalez, C.; Pople, J. A. *Gaussian 03*, revision B.02; Gaussian, Inc.: Wallingford, CT, 2004.

(42) Svozil, D.; Jungwirth, P. *J. Phys. Chem. A* **2006**, *110*, 9194.
(43) Sadhukhan, S.; Munoz, D.; Adamo, C.; Scuseria, G. E. *Chem. Phys. Lett.* **1999**, *306*, 83.
(44) Lawrence, C. P.; Nakayama, A.; Makri, N.; Skinner, J. L. *J. Chem. Phys.* **2004**, *120*, 6621.
(45) Rega, N.; Iyengar, S. S.; Voth, G. A.; Schlegel, H. B.; Vreven, T.; Frisch, M. J. *J. Phys. Chem. B* **2004**, *108*, 4210−4220.
(46) Petersen, M. K.; Iyengar, S. S.; Day, T. J. F.; Voth, G. A. *J. Phys. Chem. B* **2004**, *108*, 14804−14806.
(47) Press, W. H.; Teukolsky, S. A.; Vetterling, W. T.; Flannery, B. P. *Numerical Recipes in C*; Cambridge University Press: New York, 1992.
(48) Marinica, D. C.; Gregoire, G.; Desfrancois, C.; Schermann, J. P.; Borgis, D.; Gaigeot, M. P. *J. Phys. Chem. A* **2006**, *110*, 8802.
(49) Gaigeot, M. P.; Vuilleumier, R.; Sprik, M.; Borgis, D. *J. Chem. Theory Comput.* **2005**, *1*, 772.
(50) Tobias, D. J.; Jungwirth, P.; Parrinello, M. *J. Chem. Phys.* **2001**, *114*, 7036.
(51) Egorov, S. A.; Rabani, E.; Berne, B. J. *J. Chem. Phys.* **1998**, *108*, 1407.
(52) Bowman, L. E.; Palmer, B. J.; Garrett, B. C.; Fulton, J. L.; Yonker, C. R.; Pfund, D. M.; Wallen, S. L. *J. Phys. Chem.* **1996**, *100*, 18327.
(53) Grossman, J. C.; Schwegler, E.; Draeger, E. W.; Gygi, F.; Galli, G. *J. Chem. Phys.* **2004**, *120*, 300−311.
(54) Schwegler, E.; Grossman, J. C.; Gygi, F.; Galli, G. *J. Chem. Phys.* **2004**, *121*, 5400−5409.
(55) Groenewold, G.; Gianotto, A.; Cossel, K.; VanStipdonk, M.; Moore, D.; Polfer, N.; Oomens, J.; deJong, W.; Visscher, L. *J. Am. Chem. Soc.* **2006**, *128* (14), 4802−4813.
(56) Moore, D. T.; Li, X.; Iyengar, S. S. manuscript in preparation.
(57) Iyengar, S. S. *Theo. Chem. Accts.* **2006**, *116*, 326.
(58) A "Distributed approximating functional"-based Heaviside function[57] is used to de-noise the spectrum when necessary.
(59) A temperature dependent Boltzmann average of the frequencies in Figure 2 also shows maximal changes in the region corresponding to the four-coordinated oxygen.